INNSPUB

Journal of Biodiversity and Environmental Sciences (JBES)
ISSN: 2220-6663 (Print) 2222-3045 (Online)
Vol. 22, No. 4, p. 104-117, 2023
http://www.innspub.net

RESEARCH PAPER OPEN ACCESS

# Novel biosynthesized nanosilver impregnated heat modified montmorillonite clay K10 nanocomposites for adsorption of malachite green from aqueous solution

**M. Revathy[1], C. Aswathy[1], S. Amutha[1], E. Amutha[1], T. Madhumitha[1], E. Pushpalakshmi[1], R. Venkateshwari[1], S. Rajaduraipandian[2], G. Annadurai[*1]**

[1]*Sri Paramakalyani Centre of Excellence in Environmental Sciences, Manonmaniam Sundaranar University, Alwarkurichi, India*

[2]*Sri Paramakalyani College, Manonmaniam Sundaranar University, Alwarkurichi, India*

Article published on April 19, 2023

**Key words:** Nano silver, Montmorillonite, Nanocomposites, Malachite green, Langmuir and Freundlich, Isotherm and Kinetic studies

**Abstract**

We report here the preparation of highly stabilized nanosilver (AgNp) impregnated clay composites by the biological method. Characterizations by various techniques indicate that the silver nanoparticles were intercalated into montmorillonite clay k10 (MMT k10) composite. The adsorption of malachite green dye onto silver nanoparticles impregnated clay (Ag/MMT K10) and calcined clay (Ag/CMMT K10) in aqueous solution was investigated. Experiments were performed out as function of different dosages (1-3g/L). pH (4.7, 6.7 and 8.7) and temperature (30-60$^{o}$C).The equilibrium adsorption data of cationic dye on both (Ag/MMT K10) and calcined clay (Ag/CMMT K10) were investigated by Langmuir and Freundlich models. The maximum adsorption capability (k) has been found to be 34.3- 44.3mg/g. High adsorptive nature of the calcined clay Ag/CMMT K10 provided reasonable dye removal capacity. The kinetics of cationic dye adsorption suitably followed the pseudo- first and second order rate expression which shows that intraparticle diffusion plays an important role in the mechanism of adsorption. The experimental results indicate that calcined clay Ag/CMMT K10 is potential material for adsorption of cationic dye from aqueous solutions.

***Corresponding Author:** G. Annadurai ✉ gannadurai@msuniv.ac.in

## Introduction

Water pollution has become a worldwide environmental concern due to the removal of noxious pollutants/dyes in water bodies. Environmental pollution, in specific water pollution has turn out to be a severe problem owing to the rapid growth of industries (Fan *et al.,* 2015). Although a lot of research has been executed to expand efficient treatment technologies for polluted waters containing dyes, no specific answer has been acceptable for remediating the wide variety of textile waste (Annadurai *et al.,* 2002a; 2002b). Among several methods involve coagulation, flocculation, electro coagulation and adsorption; adsorption is currently an effective and cheap method for the elimination of dyes from water (PanelIndra Deo Mall *et al.*, 2005). Malachite green a basic, cationic, tri-phenyl methane dye, has been extensively employed for the dyeing of leather, wool, jute, silk, distilleries, food colouring agent, food additive, and also functions as fungicide, ectoparasiticide as well as antiseptic in aquaculture industry. Release of Malachite green (MG) into the hydrosphere can cause genotoxic, mutagenic, teratogenic, carcinogenic effects and it gives away the adverse colour of water as well diminishes the penetration of sunlight (Shrivastava *et al.,* 2009; Bhattacharyya and Sharma, 2005). Nanocomposite is defined as a multiphase solid substance of single phase having one, two, or three dimensions of less than 100 nanometre in range. Metal nanoparticles affixed on solid substrates suggest a broad application area such as quantum dots, solar batteries, catalysts, photo catalysts, antibacterial substances and sensors (Valaskova *et al.,* 2008; Abdel-Mohsena *et al.,* 2014).

Due to the high ion exchange capacity, high surface area, sorptive ability, negative surface charge, chemical inertness as well as less toxicity in clays (Ohashi, *et al.,* 1998; Zhao *et al.,* 2006), Zeolites (Top, 2004; Rivera-Garza *et al.,* 2000) and other alunimosilicates (Dizman *et al.,* 2007) have been used as carrier with high quality outcome (Carretero, 2002). Montmorillonite is a swelling clay mineral; 2:1 type aluminosilicate consisted of replacing negatively charged alumino silicate layers with exchangeable counter ions situated among each layer (Sposito *et al.,* 1999). The isomorphous replacement of $Al^{3+}$ for $Si^{4+}$ as well as $asmg^{2+}$ for $Al^{3+}$ in the octahedral layer results in net negative charge on the surface of the clay. Surface negative charge inequity is balanced by replaceable cations as well as the corresponding layers in this constitution are connected in concert by weak electrostatic forces (Grim and Guven, 1978). *Andrographis paniculata* is a prioritized medicinal plants regarded as king of bitters belongs to the family Acanthaceae and the extract of this plant exhibits anti-typhoid, antifungal activity, antioxidants, anti-inflammatory, anti-snake venom, antipyretic properties and immune stimulating system (Aliyu *et al.,* 2007; Puri *et al.,* 1996). Biological synthesis of silver nanoparticles is cost effective and environmental friendly in nature. It have been explored that metallic ion replaced montmorillonite scattered in water draws and adsorb negative charged bacteria enhancing germicidal properties of the substance as well as potent adsorbent for dyes, charged or non-charged organic molecules similar to Aflatoxins, herbicides, fungicides and salicyclic acid (Hu and Xia, 2006; Lombardi *et al.,* 2003; Damonte *et al.,* 2007; Jaynes *et al.,* 2007; Bonina *et al.,* 2007). However, to our best knowledge, there is no literature directing on the adsorption ability of cationic dye onto bionanocomposites based on nanosilver intercalate thermally modified clay. Therefore bionanocomposites reported in this paper can render an effective method for management of dye industry waste water.

## Material and methods

Basic dye utilized in this study was malachite green purchased from Sigma-Aldrich. Montmorillonite k10 and Silver nitrate were obtained from Hi media laboratories, Mumbai.mg has molecular formula $C_{16}H_{18}N_3ClS$ (Mol. Wt 319.85 g/mol). The maximum wavelength of this dye is 615 nm. The dye stock solution was prepared by dissolving exactly weight dye in double distilled water to the concentration of 1g/L. The experimental solutions were attained by diluting the dye stock solution in precise amount to required initial concentrations.

*Preparation of adsorbent*

*Andrographis paniculata* leaves were collected from Manonmaniam Sundaranar University campus Tirunelveli (District), Tamil Nadu, India. The collected fresh leaves were washed thrice with tap water thoroughly and twice with double distilled water in order to eliminate dust particles and other associated pollutants. About 10 grams of surface sterilized leaves were finely chopped into small slices and boiled with double distilled water for about 10-15 minutes at 60°C as shown in Fig. 1.

Then the boiled extracts were filtered using Whatmann no 1 filter paper. Calcination is the process involves heating of the material at 750°C for 3 hours. For the nanocomposite synthesis 3 g of montmorillonite clay sample and calcined clay sample was dispersed separately in 1mM aqueous silver nitrate solution and stirred for 2- 3 hours. Then 10mL of *Andrographis paniculata* leaf extract was added to the clay and calcined clay dispersed in silver nitrate solution and stirred for 24 hours.

The precipitated nanocomposites were separated through repeated centrifugation followed by washed with double distilled water. Finally obtained nanocomposites were kept for drying in hot air oven for 24 hours at 80°C. Then the dried nanocomposites were grinded well with pestle and mortar as well as stored in a freezer for further analysis.

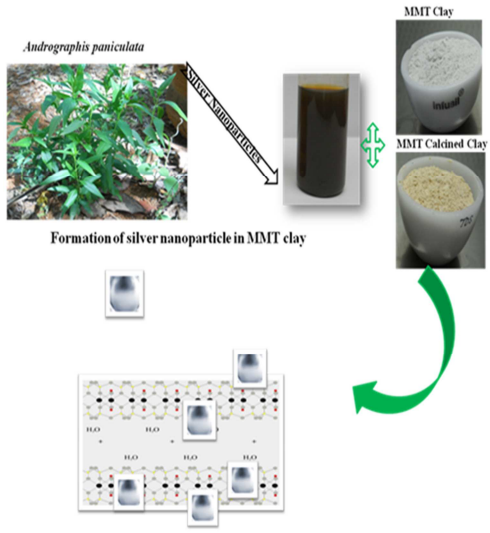


**Fig. 1.** Sample preparation and analysis.

*Characterization Studies*

The UV-visible spectrum of the composites was measured using a Perkin Elmer Lambda double beam UV-Spectrophotometer in a range of wavelengths ranging from 300-700 $nm^{-1}$. Structural analysis of the nanocomposites powder was carried out using XRD (Philips PW 1830) in the 2θ range of 10°-80° at room temperature (RT). The functional group present in the nanocomposites was scrutinized by the SHIMADZU instrument along with the sample as KBR pellet in the wave number region of 500-4,000$cm^{-1}$. Morphological characterization was performed by using Scanning Electron microscopy (Philip modelcm, 200).

*Adsorption experiments*

To investigate the effect of essential factors like pH, dosages and temperature on the adsorptive removal of cationic dye, batch experiments were performed. For every experimental run, 100ml of dye solution of known concentration, known pH and a known amount of the adsorbent were obtained in a 200mL stoppered conical flask. Effect of pH was investigated over a pH range from 4.7-8.7. The pH adjustments were performed by addition of 0.1 M HCL or NaOH using Elico pH meter (digital model). The mixture was agitated in a temperature controlled shaker at a constant speed at 180 rpm. Samples were evaluated at particular time period. Whatmann filter paper used for eliminating the suspended material and residual malachite green concentration was estimated. Dye removal efficiency on nanocomposites was estimated by the mass balance relationship (Eq. (1).

$$q_e = \frac{C_I - C_F}{m} \times v \quad (1)$$

Where, $q_e$ = Adsorption capacity (mg/g), V=Solution volume of dye (L), $C_I$ = Initial concentration of dye (mg/g), $C_F$ = Final concentration of dye (mg/g), M=Mass of adsorbent (g). The kinetic experiments procedures were principally equal to those of equilibrium tests. The aqueous samples were taken at predetermined time gap, and concentrations of dyes were identically calculated.

**Results and discussions**

The UV- visible absorption spectra of Ag Nps impregnatedmmTk10 prepared by biological method is shown in Fig 2. Notably, a single peak obtained at 421 nm in the UV visible spectrum (Fig. A & B) of the both nanocomposites occurs because of surface plasmon vibrations of silver atoms. The spectrum shown here is after 3 months of storage in normal environmental conditions. These absorption bands were most probably resulting to the Ag- NPs smaller than 30 nm (Bhattacharya *et al.,* 2014).

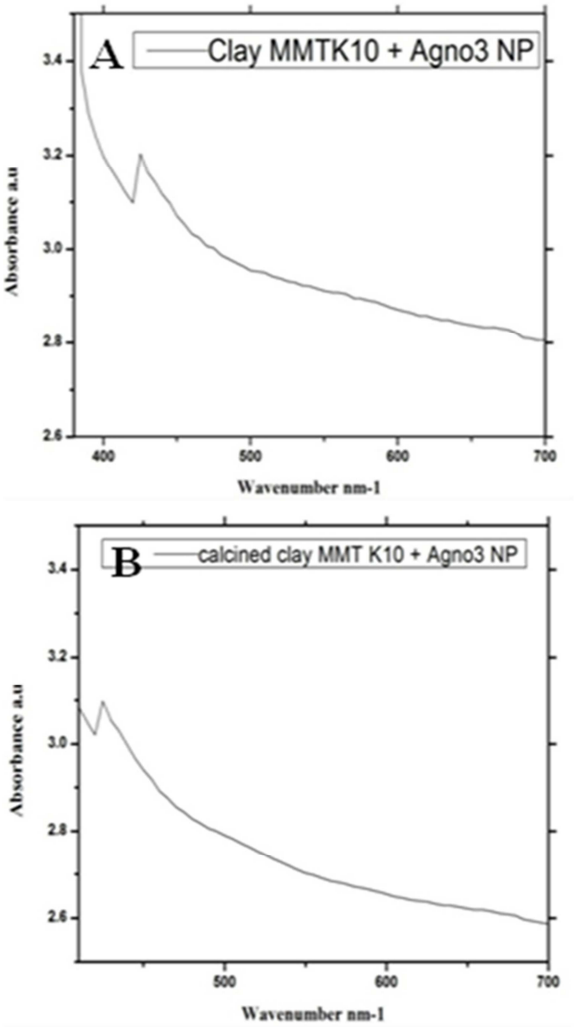


**Fig. 2.** UV- Visible spectrum for Ag/MMT k10 and Calcined Ag/MMT k10 composite.

AgNps of small sizes were impregnated into the interlamellar space ofmmTk10 utilizing biological reduction method. The color of the prepared composites gradually changed into brown color indicating the development of Ag- NPs in themmTk10 suspension. The results were also indicates that the *Andrographis paniculata* extract could be a potent stabilizer for synthesis of silver nanoparticles.

*XRD analysis*

Ag/MMTK10 composites have revealed 24 distinct peaks and Ag/CMMTK10 have revealed 29 distinct peaks in the entire spectrum of 2θ values of ranging from 20° to 80° at room temperature. The clear and strong peaks around 2 values of 35, 41, and 61 are associated to benign Ag crystalline arrangement in the compound which stabilized by Phytochemical in *Andrographis paniculata* extract as shown in Fig.3. The XRD models obviously display the occurrence of silver nanoparticles in nanocomposite forms by Vaidyanathan *et al.,* 2007.

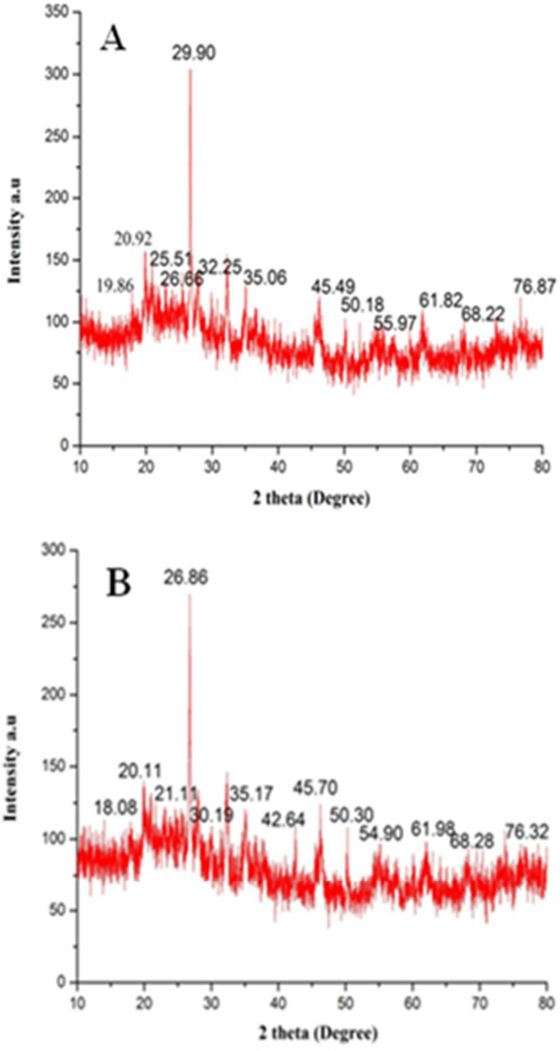


**Fig. 3.** XRD Spectrum of A)Ag/MMT K10 and B)Ag/CMMK10 nanocomposites.

It was also noticed that both Ag/MMT K10 and Ag/CMMT K10 illustrated highest peak intensity and have good crystalline characters by Hanifehpour *et al.,* 2012. The obtained results implied the successful formation of dispersion of silver nanoparticle on the montmorillonitek10 matrix. The similar particles obtained by xrd of silver clay starch bionanocomposites (Mansor Bin Ahmad *et al.*, 2010), copper, gold intercalated montmorillonite, (Dietrich and Anthony Dipak kumar, 2011).

*FTIR analysis*

The band which appeared at 798.89cm$^{-1}$ was corresponding to the =C-H bending of the functional group alkenes. FTIR also shows peak at 1042. 19cm$^{-1}$ was arises due to the presence of C-N stretching of the functional group aliphatic amines. The number of functional group present in the Ag/MMT K10 contains low number when compared to Ag/CMMT K10 composite as shown in Fig. 4. While the clay molecules expands the interstitial layers present in the clay also expands due to the process of calcination and thus hold more functional groups (Cheng *et al.*, 2005).

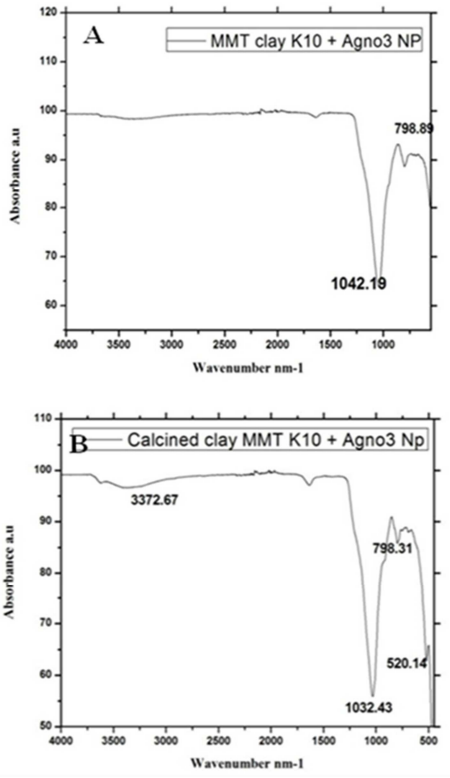


**Fig. 4.** FTIR Spectrum of A)Ag/MMT K10 and B)Ag/CMMT K10 nanocomposites.

The presence of functional group is also one of the important factors in the adsorption mechanism. The absorption peak at around 3372cm$^{-1}$ was due to N-H stretching of the functional groups 1$^{o}$, 2$^{o}$ amines and amides. The peak obtained at 1032.43cm-1 was ascribed to the presence of the functional group aliphatic amines. The IR band obtained in Ag/CMMT K10 nanocomposite at 798cm -1 was ascribed to the C- Cl stretching of alkyl halides by Zaitsev *et al.,* 1990. The band appeared at 520cm$^{-1}$ C- Br stretching of the functional group alkyl halides. Similar results were noticed in schizophyllan silver nanoparticle composite by Abdel-Mohsen *et al* in 2014.

*SEM analysis*

The surface morphology of the synthesized nanocomposites was shown in the Fig.5. Small sized particles are bound aggregates due to the intermolecular forces of clay composite in both Ag/MMTK10 and Ag/CMMTK10 nanocomposite. Silver nanoparticles were bind over the sheet like surface of the clay and calcined clay nanocomposites. Similar results were obtained in Studies on Preparation and analysis of Organoclay Nano Particles by the authors Bhattacharya S.S. and Mandot Aadhar in the year 2014; Shrivastava *et al.,* 2009; Zaitsev *et al.,* 1999).

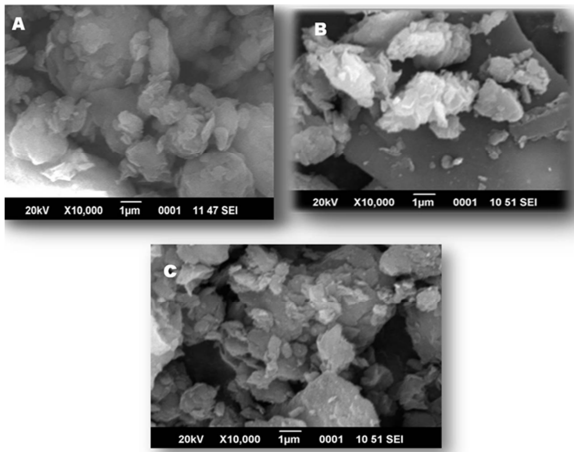


**Fig. 5.** SEM Image of a)mmT K10 b) AG/MMT K10 and c) AG/CMMT K10 nanocomposite.

After biological modification with Silver nanoparticles, flakes were attached by functional features to form aggregates as revealed in Fig. 5a, b and c.

When Ag ions are substituted by other cations inmmTk10, the limit among the interlayer in Ag/MMTk10 and Ag/CMMTK10 nanocomposite is more evident than that of interlayer inmmTK10 signifying the Ag ions may increase the distance between the tetrahedral sheets and modify the structure of mmT K10 by Cheng *et al.,* 2005.

*Effect of Dosages*

The effect of adsorbent dosages on Malachite Green uptakes by (Ag-CMMTK10 Clay) for three different dosages sizes is shown in (Fig 6a). It can be surveyed that as the dosages increases, the adsorption of dye increases. The results confirm that there is a slow increase in adsorption with increasing dosages. Such an effect of possibly by reason of the inability of the large dye molecule to penetrate all the internal pore structure of the (Ag-CMMTK10 Clay) and similar phenomenon was described earlier for the adsorption of certain dyes on various adsorbents (Tsai *et al.,* 2001; Sivaraj *et al.,* 2001; Annadurai *et al.,* 2002; Yoshida *et al.,* 1993; Kawamura *et al.,* 1993).

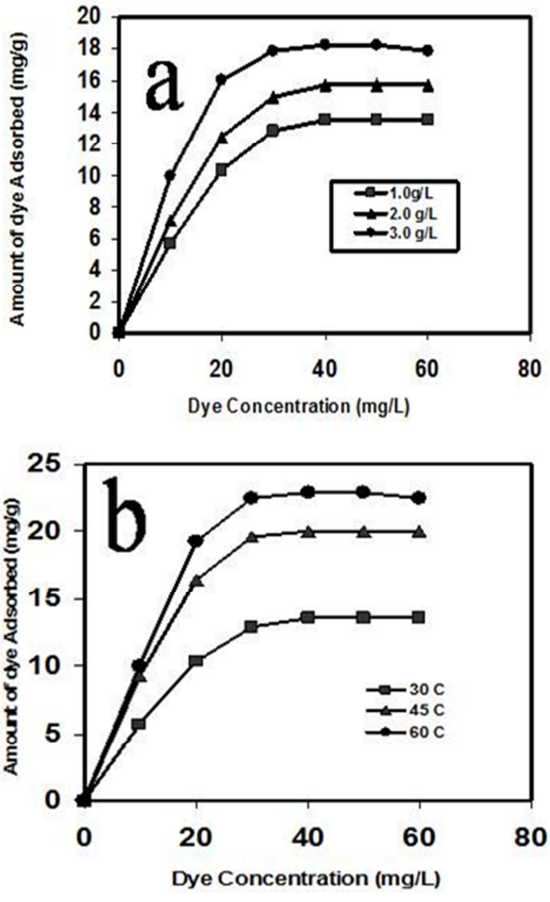


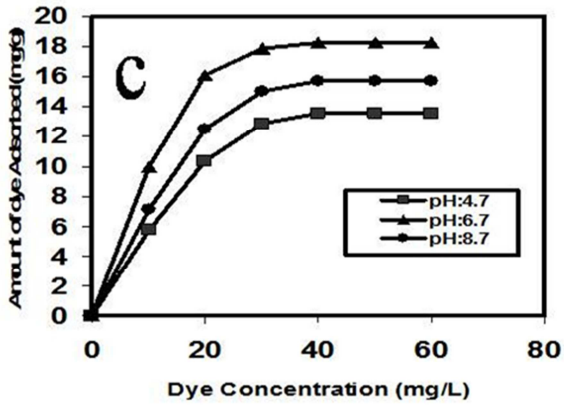


**Fig. 6.** Effect of a) adsorbent dosages, b) temperatures and c) $p^H$ on malachite green dye.

Dye adsorption increases with increases in adsorbent dosages because of more number of surface active sites present on the surface for the malachite green dye adsorption on the Ag/MMTk10 nanocomposites. Primarily the dye removal rate is increased quickly then declined as the dose increased. Due to the availability of the free sites the dye removal percentage is higher and faster in the initial stage and increase in uni molecular layers. As per the obtained results dose of adsorbent at 3.0 g/L shows the maximum removal of malachite green dye, after that there is no significant change in the dye removal though the dosage is increased.

*Effect of Temperature*

Malachite Green uptake as a function of temperature by (Ag-CMMTK10 Clay) (30, 45 and 60°C) is shown in (Fig 6b) The adsorption of dye at higher temperature was found to be better compared to that at a lower temperature. The curve denotes the strong affinity of the method for monolayer formation (Sivaraj *et al.,* 2001; Annadurai *et al.,* 2002, Yu *et al.,* 2002; Ravikumar, 2000, Muzzarelli, 1973). The increase in temperature would increase the mobility of the large dye ion and also creates a swelling effect within

The internal structure of the Ag-CMMTK10 Clay, thus enabling the large dye molecule to enter further for studies (Muzzarelli, 1973). Consequently, the adsorption ability should mostly depend on the chemical interaction among the functional groups on the adsorbent surface and the adsorbate and should

increase with temperature rising (Kawamura *et al.,* 1993). Retardation in the adsorption takes place while the temperature rises from 30 to 60°C. This occurs due to the fact that the adsorbate solubility increases at higher temperature and decrease in chemical potential. When the temperature increases, pores of the adsorbent molecules increases with diffusion rate of the adsorbate materials across the outer boundary layer also increases. Temperature change will alter the equilibrium ability of the adsorbent changes for the specific adsorbate

*Effect of pH*

Fig. 6c shows the effect of pH on adsorption of the cationic dyes onto cross-linked (Ag-CMMTK10 Clay). In common, uptakes were much superior in acidic solutions than those in neutral and alkaline conditions. At lower pH more protons will be obtainable to protonate amino groups of molecules to form groups $-NH^{3+}$, in that way increasing the electrostatic attractions between negatively charged adsorption sites and positively charged dye cation and causing an increase in dye adsorption. This description corresponds with our data on pH effect. It can be found that the pH of aqueous solution takes place an important part in the adsorption of cationic dyes onto (Ag-CMMTK10 Clay). pH is the major parameter which influences the adsorbent process on the adsorbent. The optimum pH for the maximum dye removal was achieved at pH 6.7 and maximum 18mg/L of the dye desorption takes place at this pH.

*Langmuir isotherms*

In the current research, the equilibrium data were investigated according to the linear form of Langmuir Eq. (2) Freundlich Eq. (3) and model of adsorption isotherm. The Langmuir isotherm has found profitable appliance too many other real sorption processes and it can be used to elucidate the sorption of Malachite Green onto (Ag-CMMTK$_{10}$ Clay). A fundamental hypothesis of the Langmuir theory is that sorption takes place at particular sites within the adsorbent (McKay, 1984; Low and Lee, 1997; Wei *et al.,* 1992). The data attained from the adsorption experiment performed in the recent survey was fitted in different adsorbent dosages, pH and temperature in isotherm equation. The saturation monolayer can be denoted by the expression.

$$q_e = \frac{KbC_e}{(1 + bC_e)} \quad (2)$$

$$\frac{1}{q_e} = \frac{1}{K} + \frac{1}{KbC_e} \quad (3)$$

A plot of (1/qe vs 1/Ce) resulted in a linear graphical relation signifying the applicability of the above model as shown in (Fig.7 a to c). The values are evaluated from the slope and intercept of different straight line corresponding to the different dosages, pH and temperature (b) energy of adsorption and (k) adsorption capacity. The Langmuir isotherm constant ($q_e$) in equation (2) is a measure of the amount of dye adsorbed, when the monolayer is concluded. Monolayer capacity (k) of the adsorbent for the dye malachite green is similar acquired from adsorption isotherm. The observed statistically significant (at the 95% confidence level) linear relationship as confirmed by the $R^2$ values (close to unity) denote the applicability of the isotherm (Langmuir isotherm) and surface. The Langmuir isotherm constants along with correction coefficients are stated on (Table 1) it is also obvious from the shape of the adsorption isotherm, that it fits in to the $L_2$ category of isotherm, which designates the normal (or) Langmuir type of adsorption, (Chiou and Hy Li, 2003; Yui *et al.,*1994; Rinaudo, 2006). Such isotherms are frequently encountered when the adsorbate has a strong intermolecular attraction for the surface of the adsorbent. The $L_2$ shape of isotherm examined in the current concern clearly implies that Malachite Green molecules must have been strongly attached to the (Ag-CMMTK10 Clay).

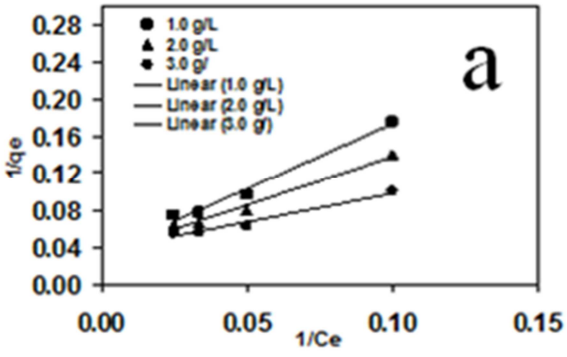

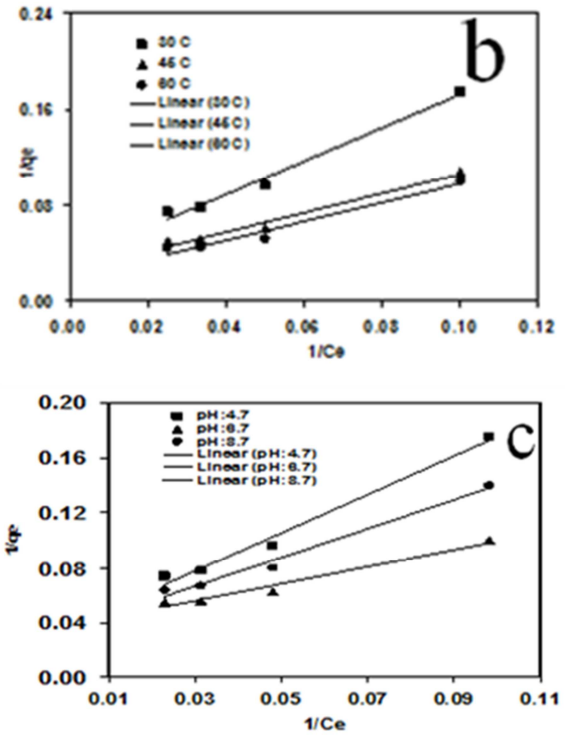


**Fig. 7.** Langmuir isotherm for the adsorption of Malachite Green dye using (Ag-CMMTK10 Clay) at different a) dosages, b) pH and c) temperatures.

*Freundlich Isotherms*

Freundlich isotherm is utilized for mixed surface energies system and the sorption isotherm is the most suitable form of denoting the experimental data at different dosages, pH and temperature (Ag-CMMTK10 Clay) as revealed in (Fig.8a-c). Langmuir and Freundlich isotherm (Eq.- 4 and 5) is suited completely the line shows excellent results in Fig. at different dosages, pH, and temperature which represents optimum adsorption illustrate in the Fig 8 (a to c) Langmuir and Freundlich isotherm satisfies which shows association of 0.0997. Malachite green dye removal takes place in two discrete stages. Comparatively rapid one is followed by

$$q_e = K_F C_e^{1/n} \quad (4)$$

$$\ln q_e = \ln K_F / (1/n) \ln C_e \quad (5)$$

The numerous constants, related with the isotherm are the intercept, which is approximately on indicator of sorption capacity (kf) and the slope (1/n) sorption intensity values are tabulated in (Table -1). Freundlich of isotherm has been pointed up to be an extraordinary situation of heterogeneous surface energies and it can be simply unlimited to this condition. It has been affirmed by Krajewska in 2005 and Kawamura *et al.,* (1997).

In the year 1997, that degree of the exponent 1/n presents a sign of the favorability and capability of the adsorbent/adsorbate system. The values n>1 signify favorable adsorption states. Generally, the exponent between 1<n<10 confirms beneficial adsorption.

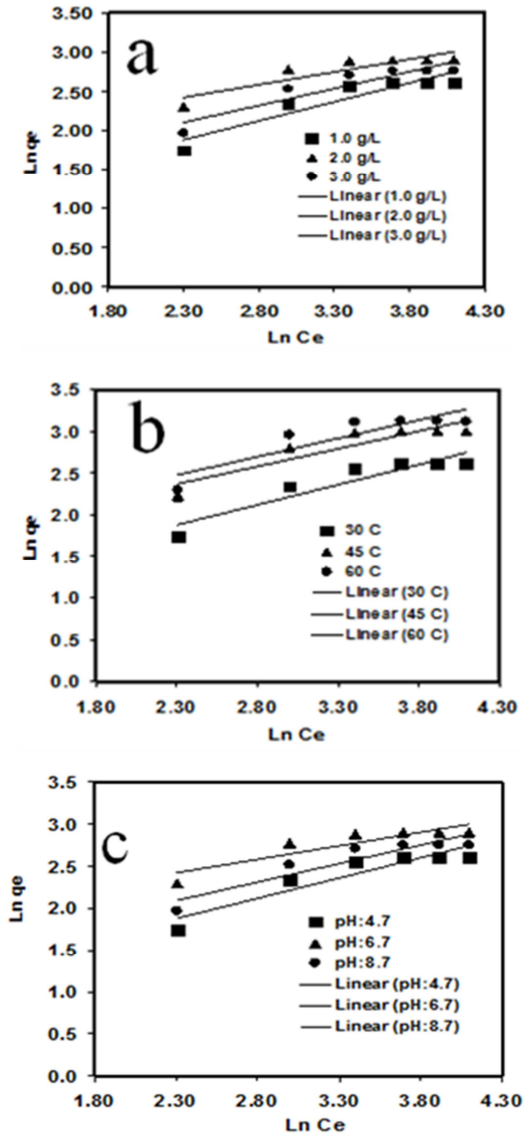


**Fig. 8.** Freundlich isotherm for the adsorption of Malachite Green dye using (Ag-CMMTK10 Clay) at different a) dosages, b) pH and c) temperatures.

This is not limited to the monolayer formation. This model envisages that dye intensity in the adsorbent will rise with increase in dye concentration in the solution. Alternatively in the Langmuir model, it is understood that intermolecular forces diminish promptly with distance and this guides to the insight that coverage by biosynthesized nanocomposite is of monolayer type. Additional, it is presumed that once a specific site of the adsorbent is engaged by an adsorbent molecule, no more adsorption happen at that site. Hypothetically, adsorbent has restricted amount of sites and formerly every sites are occupied by nanocomposite, additional adsorption cannot occur. Nevertheless, if the full concentration range is separated into three linear states, nice fits to the experimental data are recorded.

**Table 1.** Langmuir and Freundlich isotherm constants at different adsorbent dosages, temperature, and pH-Ag -cmMTK10 Clay- Malachite Green dye.

| Parameters | | Langmuir Isotherm -model parameters | Freundlich Isotherm -model parameters |
|---|---|---|---|
| Dosage (g/ L) | 1.0 | K=21.14; b= 1.12; $R^2$= 0.9748 | $K_F$=0.964;n=1.0374 ; $R^2$= 0.8534 |
| | 2.0 | K=41.88;b=1.08 ; $R^2$= 0.9489 | $K_F$=1.0249;n=0.9757;$R^2$= 0.7879 |
| | 3.0 | K=26.14;b=1.00; $R^2$= 0.9702 | $K_F$=0.7677;n=1.3022; $R^2$=0.8640 |
| Temperature (°C) | 30 | K=26.14;b=1.115; $R^2$= 0.9748 | $K_F$=0.840;n=2.008 ; $R^2$=0.8838 |
| | 45 | K=34.36b= 1.124; $R^2$=0.9535 | $K_F$=1.0597;n=1.940; $R^2$=0.8109 |
| | 60 | K=44.39; b=1.121; $R^2$=0.9721 | $K_F$=0.9452;n=1.719 ; $R^2$=0.8664 |
| pH | 4.7 | K=36.49;b=0.83; $R^2$= 0.9744 | $K_F$=0.6073;n=1.754; $R^2$=0.8838 |
| | 6.7 | K=26.14;b=1.12; $R^2$=0.9748 | $K_F$=0.9640; n=2.008;$R^2$= 0.8534 |
| | 8.7 | K=31.14;b= 0.98; $R^2$= 0.9714 | $K_F$=0.8442;n=1.9047; $R^2$=0.8580 |

This is almost certainly (i) due to the existence of different groups such as aluminium, silica in the (Ag-CMMTK10 Clay) dye molecule producing uneven energy distribution in the nanocomposite (Ag-CMMTK10 Clay) surface or (ii) by a solely physical adsorption. The general shape of the isotherm curve comprising pointed curvature close to the saturation position and short equilibrium time are also especial characteristics of Langmuir equilibrium with maximum sorption capacity. The investigational conclusions also corroborated the saturation ability expected by Langmuir equation at different dosages, pH and temperatures.

*Adsorption Kinetics: Malachite Green: (Ag-CMMTK10 Clay)*

The kinetics of adsorption was analyzed for its potential significance in the management of dye containing industrial effluents. Various kinetic models have been estimated to explain the process by which pollutants are adsorbed.

To study the method of the dye adsorption kinetic models were measured as follows. The kinetics of adsorption is vital from the viewpoint that it governs the process efficiency. Numerous kinetic models have been utilized by several workers and diverse structures agrees with different models but the Langergrens rate equations for the sorption of a solute form liquid solution. In order to check the controlling mechanism of adsorption processes such as group transport and chemical reaction, a number of kinetic models are exploited to investigate experimental data. The effect of adsorbent was various weights of dosages on sorption of Malachite Green as exposed in Fig. (9a). It can be observed that as the dosages increases, the adsorption of dye increases. The results demonstrate that there is a steady increase in adsorption with increasing dosages.

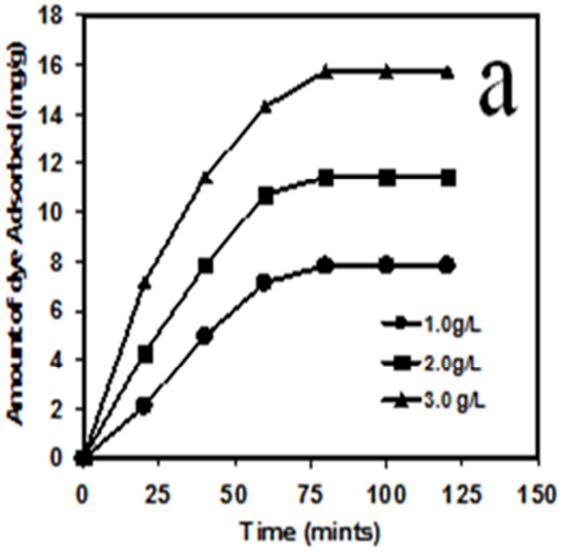

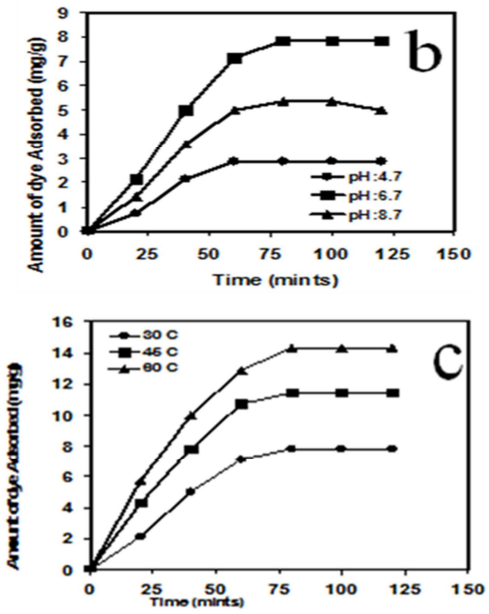


**Fig. 9.** Effect of specific dye (Malachite Green) uptake a) at different dosages b) at different p$^{H}$ and c) at different temperature with time (mts).

The consequence of pH on adsorption process was scrutinized at different pH values, namely, 5.7, 6.7 and 8.7 and the results are represented in (Fig 9 b). This might be owing to the number of positive charges on the sorbent surface which directs to the no rejection of the negatively charged dye molecule, and thus increasing the adsorption. In common, the uptakes are much elevated in acidic solutions than those in neutral and alkaline conditions. The highest values of the adsorption capability proportion between acidic and alkaline states reach 5.7 to 8.7 malachite Green (Ag-CMMTK10 Clay) sorbent. The dye absorption could additionally gain support from the ion exchange reaction. This justification coincides with our information on pH effect. It can be observed that the pH of aqueous solution acts a key role in the adsorption of malachite Green (Ag-CMMTK10 Clay) sorbent.

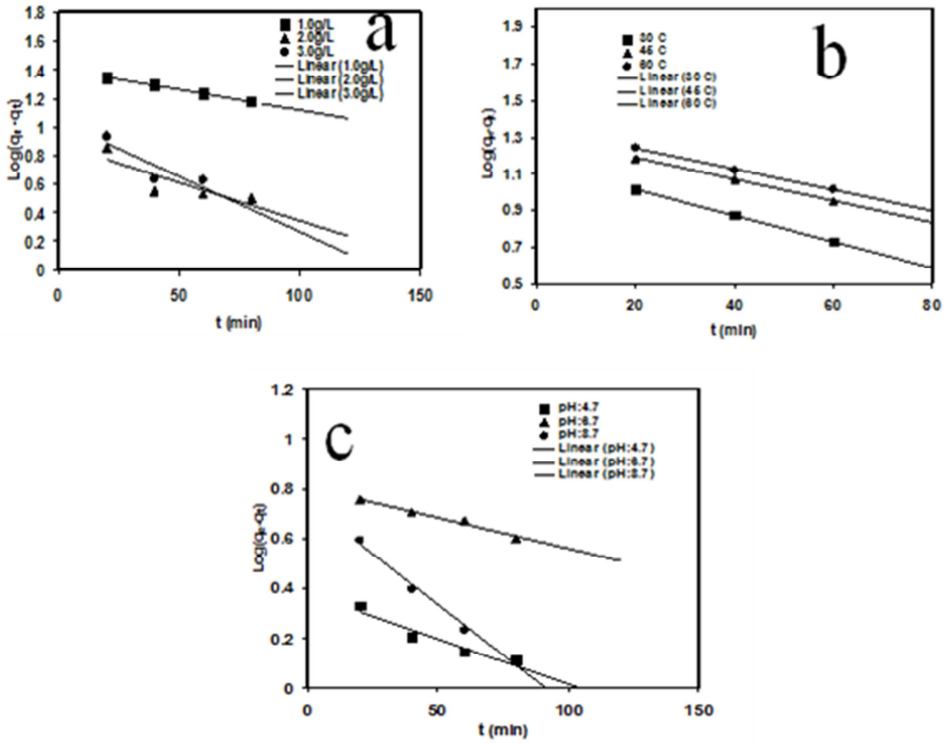


**Fig. 10.** Effect of specific dye (Malachite Green) uptake a) at different adsorbent dosages with time (mts)b) at different temperatures with time(mts) c) at different pH with time (mts) in the pseudo-first-order equation

The increase in temperature would increase the mobility of the bulk dye ion as well as creates a swelling effect in the interior arrangement of the Environmental Nanomaterial, therefore permitting the large dye molecule to penetrate further as shown in (Fig 9c)(Mckay *et al.,* 1984; Fan *et al.,* 2015). Hence, the adsorption ability must predominantly depend on the chemical interaction among the

functional groups on the adsorbent surface and the adsorbate and should increase with rise in temperature (Aguiar *et al.,* 2017; Chang and Juang, 2004). From a technique design perspective, a mass investigation of adsorption rates is consequently satisfactory to functional operation as shown in (Fig 10 a to c). A simple kinetic investigation of adsorption is the pseudo-first-order equation;

$$\frac{dq_t}{q_t} = K_1(q_{eq} - q_t) \quad (6)$$

Following distinct integration by applying the initial conditions $q_t$=0 at $t$=0 and $q_t$=$q_t$ at $t$=$t$, equation (6) be converted into;

$$\log (q_{eq} - q_t) = \log q_{eq} - \frac{K_1}{2.303} t \quad (7)$$

Where $q_{eq}$ and $q_t$ are quantity of dye adsorbed at equilibrium as well as at time, inmg g-1 subsequently, and $K_1$ is the first order rate constant, was employed to the current studies of dye adsorption. As such the values of log ($q_e$-$q_t$) vs t were estimated from the kinetic records of (Eq-7) and designed against time.

The first-order rate constant evaluated from the plots are exposed in (Table 2 and 3). Adsorption kinetics for certain scheme can also be depicted by a pseudo-second order reaction (Sivaraj *et al.,* 2001; Peternel *et al.,* 2007).

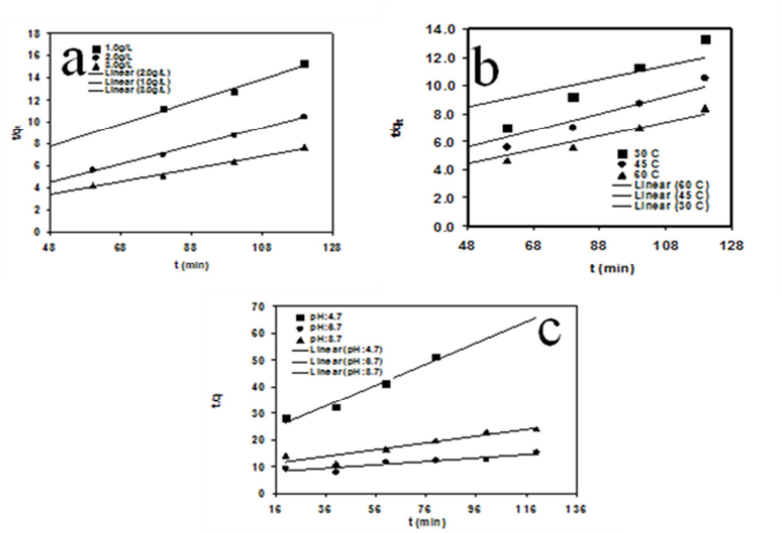


**Fig. 11.** Effect of specific dye (Malachite Green) uptake a) at different adsorbent dosages with time (mts) b) at different temperatures with time (mts) c) at different pH with time (mts) in the pseudo-second-order equation

The pseudo-second-order equation depend on adsorption equilibrium capacity can be expressed in the form;

$$\frac{dq_t}{q_t} = K_2(q_{eq} - q_t)^2 \quad (8)$$

Where $k_2$ is the rate constant of pseudo-second-order adsorption. Combining equation (9) and relating the initial conditions, we have

$$\frac{1}{(q_{eq} - q_t)} = \frac{1}{q_e} + K_2 t \quad (9)$$

or consistently,

$$\frac{t}{q_t} = \frac{1}{K_2 q_{eq}^2} + \frac{1}{q_e} t \quad (10)$$

The kinetics studies of dye adsorption on Ag/CMMTk10 nanocomposite have been examined by applying various first and second order kinetic equations correlated with time.The values of pseudo first order and second order rate constant and all the linear coefficient are found to be statistically significant as shown in (Fig. 11 a-c).This indicates the pseudo order equations are applicable.

The $K_1$ and $K_2$ values obtained from the Langergran equations for the adsorbent are almost equal to the value represented in the Table 2. Estimated correlations are closer to unity for first order kinetics model. Hence the adsorption dynamics could fitted more suitable by first order kinetic model for dye adsorption. The $k_2$ (mg $g^{-1}$ $min^{-1}$) and $q_{eq}$ (mg $g^{-1}$ $min^{-1}$) vaues as calculated are listed in Table 2.

**Table 2.** Pseudo-first order rate constant at different dye concentration, pH and temperature Ag - cmMTK10 Clay -Malachite green dye.

| Pseudo-first order | | Pseudo-first-order rate constant |
|---|---|---|
| Dye Concentration (mg/L) | 20 | $K_1$=0.0658;$q_{eq}$=1.4165 $R^2$= 0.99989 |
| | 40 | $K_1$= 0.258; $q_{eq}$= 1.5401; $R^2$= 0.9999 |
| | 60 | $K_1$= 0.226; $q_{eq}$= 1.4597;$R^2$= 0.9989 |
| pH | 5.5 | $K_1$=0.0258;$q_{eq}$= 1.4165; $R^2$= 0.9989 |
| | 6.8 | $K_1$=0.0257;$q_{eq}$= 1.5401; $R^2$= 0.9999 |
| | 7.8 | $K_1$=0.0258;$q_{eq}$= 1.4597; $R^2$= 0.9896 |
| Temperature (°C) | 30 | $K_1$=0.0257;$q_{eq}$= 1.4165; $R^2$= 0.9989 |
| | 45 | $K_1$=0.0287;$q_{eq}$= 1.5401; $R^2$= 0.9998 |
| | 60 | $K_1$=0.0218;$q_{eq}$= 1.4597; $R^2$= 0.9989 |

**Table 3.** Pseudo- second order rate constant at different dye concentration, pH and temperature Ag - cmMTK10 Clay -Malachite green dye.

| Pseudo second Order Type - I | | Pseudo second order rate constant |
|---|---|---|
| Dye Concentration (mg/L) | 20 | $K_2$= 0.0442; $q_{eq}$= 14.51; $R^2$= 0.9989 |
| | 40 | $K_2$= 0.0075; $q_{eq}$= 34.96; $R^2$= 0.9986 |
| | 60 | $K_2$= 0.0156; $q_{eq}$= 27.47; $R^2$= 0.9987 |
| pH | 5.5 | $K_2$= 0.0154; $q_{eq}$= 23.14; $R^2$= 0.9995 |
| | 6.8 | $K_2$= 0.0155; $q_{eq}$= 26.24; $R^2$= 0.9996 |
| | 7.8 | $K_2$= 0.0156; $q_{eq}$= 27.47; $R^2$= 0.9997 |
| Temperature (°C) | 30 | $K_2$= 0.1093; $q_{eq}$= 14.90; $R^2$= 0.9995 |
| | 45 | $K_2$= 0.0038; $q_{eq}$= 25.90; $R^2$= 0.9686 |
| | 60 | $K_2$= 0.0476; $q_{eq}$= 21.08; $R^2$= 0.9935 |

## Conclusion

Thus, we offer a simple fragile strategy to synthesize Ag Nanoparticles impregnated clay and calcined claymmTk10 nanocomposites. The experimental studies have signified that Ag/MMTk10 and Ag/CMMTk10 has the higher capacity to behave as an adsorbent for the removal of malachite green from aqueous solutions. In addition, the adsorption isotherm can be best denoted by a Langmuir and Freundlich models.

The experimental results indicated that Ag/CMMT possessed a maximum dye adsorption capacity for malachite green. The dye uptake rate by bionanocomposites nicely followed pseudo-first order kinetic model compared with pseudo first order kinetic model. The high adsorption capacity of the nanocomposites can be attributed to the strong attraction between the charges of the claymmTk10 and cationic dye. Consequently, the adsorption process as well as the bionanocomposites presented in this research may afford a potential and low cost material for removing toxic dyes from wastewater.

## References

**Abdel-Mohsena G, Rasha M, Abdel-Rahman C, Moustafamg, Foudab L, Vojtovaa L, Uhrovad AF, Hassane Salem S, Al-Deyabb Ibrahim E, El-Shamyf Jancara J.** 2014. Preparation, characterization and cytotoxicity of schizophyllan/silver nanoparticle composite. Carbohydrate Polymers **102,** 238-245.

**Aguiar JE, Cecilia PAS, Tavares DCS, Azevedo ER, Castellon SMP, Lucena IJ.** 2017. Adsorption study of reactive dyes onto porous clay Heterostructures. Appl. Clay Sci **135,** 35-44.

**Aliyu B, Musa AM, Sallau MS, Oyewale AO.** 2009. Proximate Composition, Mineral Elements and Anti-nutritional Factors of *Anisopus mannii* N. E. Br. (Asclepiadaceae). Trends Appl. Sci. Res **4(1),** 68-72.

**Annadurai G, Juang RS, Lee DJ,** 2002a. Use of cellulose-based wastes for adsorption of dyes from aqueous solutions. J. Hazard Mater. **B92,** 263-74.

**Annadurai G, Juang RS, Lee DJ.** 2002b. Microbiological degradation of phenol using mixed liquors of *Pseudomonas putida* and activated sludge. Waste Management **22(7),** 703-710.

**Bhattacharya SS, Mandot Aadhar M.** 2014. Preparation and characterization of water-absorbing composite membrane for medical applications. Research Journal of Engineering Sciences **3(3),** 10-16.

**Bhattacharyyakg D, Sharma A.** 2005. Kinetics and Thermodynamics of Methylene Blue Adsorption on Neem (*Azadirachta indica*) Leaf Powder. Dyes and Pigments **65(1),** 51-59.

**Bonina M, Giannossi L, Medici C, Puglia V, Summa Tateo F.** 2007. Adsorption of salicylic acid on bentonite and kaolin and release experiments. Appl. Clay Sci **36,** 77-85.

**Carretero MI.** 2002. Clay minerals and their beneficial effects upon human health. A review. Appl. Clay Sci **21,** 155-163.

**Chang MY, Juang RS.** 2004. Adsorption of tannic acid, humic acid, and dyes from water using the composite of chitosan and activated clay. Journal of Colloid and Interface Science **278,** 18-25.

**Cheng FY, Su CH, Yang YS, Yeh CS, Tsai CY, Wu CL**. 2005. Characterization of aqueous dispersions of Fe3O4 nanoparticles and their biomedical applications. Biomaterials **26,**729-738

**Chiou MS, Li HY.** 2003. Adsorption Behavior of Reactive Dye in Aqueous Solution on Chemical Cross Linked Chitosan Beads. Chemosphere **50,** 1095-1105.

**Damonte M, Torres Sanchez RM, Dos Santos Afonso M.** 2007. Some aspects of the glyphosate adsorption on montmorillonite and its calcined form. Appl. Clay. Sci. **36,** 86-94.

**Dietrich K, Anthony JS.** 2011. Metal Nanoparticles Stabilized on Montmorillonite Clay: Synthesis and Reactivities and Biotechnology in Food Production and Processing. Sci. & Cult. **77(11-12),** 499-502.

**Dizman BJC, Badger MO, Elasri LJ.** 2007. Mathias, Antibacterial fluoromicas: A novel delivery medium. Appl. Clay. Sci. **38,** 57-63.

**Fan Y, Liu HJ, Zhang Y, Chen Y.** 2015. Adsorption of anionic MO or cationic MB from MO/MB mixture using polyacrylonitrile fiber hydrothermally treated with hyperbranched polyehtylenimine. J. Hazard Mater **283,** 321-328.

**Grim RE, Guven N.** 1978. Bentonite: Geology, Minerology, Properties and uses Amsterdam Elevier scientific.

**Hanifehpour Y, Mirtamizdoust B, Farzam AR, Joo SW.** 2012. Synthesis and crystal Structure of $[Pb(phen)(l\text{-}N_3)(l\text{-}NO_3)]_n$ and its thermal decomposition to PbO nanoparticles. J. Magn. Magn. Mater. **22,** 957-962.

**Hu H, Xia MS.** 2006. Adsorption and antibacterial effect of copper-exchanged montmorillonite on Escherichia coli K88. Appl. Clay. Sci. **31,** 180-184.

**Jaynes JW, Zartman R, Hudnall W.** 2007. Aflatoxin Toxicity Reduction in Feed by Enhanced Binding to Surface-Modified Clay Additives. Appl. Clay. Sci. **36,** 197-205.

**Kawamura Y, Yoshida H, Asai S.** 1997. Effects of chitosan concentration and precipitation bath concentration on the material properties of porous crosslinked chitosan beads. Sep. Sci. Technol. **32,** 1959-1974.

**Kawamura YM, Mitsuhashi, Tanibe H, Yoshida H.** 1993. Adsorption of metal ions on polyaminated highly porous chitosan chelating resin. Ind. Eng. Chem. Res. **32**, 386-391.

**Krajewska B.** 2005. Membrane-based processes performed with use of chitin/chitosan materials. Sep. Purif. Technol. **41,** 305-312.

**Lombardi B, Baschini M, Torres Sanchez RM.** 2003. Adsorption and antibacterial effect of copper-exchanged montmorillonite on *Escherichia coli* K88. Appl Clay Sci **24,** 43-50.

**Low KS, Lee CK.** 1997. Quaternized Rice Husk as Sorbent for Reactive Dyes. Bioresource Technol. **61,** 121-125.

**Mansor Bin Ahmad, Kamyar Shameli, Wan Md Zin Wan Yunus, Nor Azowa Ibrahim Majid Darroudi.** 2011. Synthesis and Characterization of Silver/Clay/Starch Bionanocomposites by Green Method. Australian Journal of Basic and Applied Sciences **4(7),** 2158-2165.

**Mckay G.** 1984. Analytical Solution Using a Pore Diffusion Model for a Psuedo- lI reversible Isotherm for the Adsorption of Basic Dye on Silica. AICHE J **30,** 692.

**Muzzarelli RAA.** 1973. Removal of uranium from solutions and brines by a derivative of chitosan and ascorbic acid. Natural Chelating Polymers. Pergamon Press, Oxford.

**Ohashi F, Oya A, Duclaux L, Beguin F.** 1998. Structural model calculation of antimicrobial and antifungal agents derived from clay minerals. Appl. Clay. Sci. **12,** 435-445.

**PanelIndra Deo Mall, Vimal Chandra Srivastava, Nitin Kumar Agarwal, Indra Mani Mishra.** 2005. Removal of congo red from aqueous solution by bagasse fly ash and activated carbon: Kinetic study and equilibrium isotherm analyses. Chemosphere **61(4),** 492-501.

**Peternel IT, Koprivanac N, Bozic AML, Kusic HM.** 2007. Comparative study of UV/$TiO_2$, UV/ZnO and photo-Fenton processes for the organic reactive dye degradation in aqueous solution. J. Hazard Mater **148(12),** 477-484.

**Puri R, Saxena RP, Saxena KC, Saxena V, Srivastava Tandon JS.** 1996 Immunostimulant Agents from *Andrographis paniculata*, J. Natural Prod **56(7),** 995-999.

**Ravi Kumar MNV.** 2000. A review of chitin and chitosan applications. React Funct Polym **46,** 1-27.

**Rinaudo M.** 2006. Characterization and properties of some polysaccharides used as biomaterials. Macromol. Sympl **245-246,** 549-557.

**Rivera-Garza M, Olgu´ın MT, Garc´ıa-Sosa I, Alcantara D, Rodriguez-Fuentes G.** 2000. Silver supported on natural Mexican zeolite as an antibacterial material. Micropor. Mesopor. Mater **39,** 431-444.

**Shrivastava S, Bera T, Singh SK, Singh G, Ramachandrarao P, Dash D**. 2009. Characterization of Antiplatelet Properties of Silver Nanoparticles. ACS Nano **3(6),** 1357-1364.

**Sivaraj R, Namasivayam C, Kadirvelu K.** 2001. Orange Peel as an Adsorbent in the Removal of Acid Violet 17 (Acid Dye) from Aqueous Solutions. Waste Manag **21,** 211-222.

**Sposito G, Skipper NT, Sutton R, Park SH, Soper AK, Greathouse JA.** 1999. Geology, mineralogy, and human welfare. Proc Natl Acad Sci **96,** 3358.

**Top S.** 2004. Silver, zinc, and copper exchange in a Na-clinoptilolite and resulting effect on antibacterial activity. Appl. Clay. Sci. **27,** 13-19.

**Tsai WT, Chang CY, Linmc, Chien SF, Sun HF, Hsieh MF.** 2001. Adsorption of Acid Dye onto Activated Carbon prepared from Agricultural Waste Bagasse by ZnCl2 Activation. Chemosphere **45,** 1245-1252.

**Vaidyanathan G, Sendhilnathan S, Arulmurugan R.** 2007. Structural and magnetic properties of $Fe_3O_4$ nanoparticles by co-precipitation method. J. Magn. Magn. Mater. **313,** 293-299.

**Valaskova M, Simha Martynkova G, Leskova J, apkova P, Klemm V, Rafaja D.** 2008. Silver nanoparticles/montmorillonite composites prepared using nitrating reagent at water and glycerol. Journal of Nanoscience and Nanotechnology **8,** 3050-3058.

**Wei YC, Hudson SM, Mayer JM, and Kaplan DL.** 1992. The Crosslinking of Chitosan Fibers. J Polym Sci, Polym Chem **30,** 2187-2196.

**Yoshida H, Okamoto A, Kataoka T.** 1993. Adsorption of acid dye on cross-linked chitosan fibers. Equilibria Chem Eng Sci **48,** 2267-2272.

**Yui T, Imada K, Okuyama K, Obata Y, Suzuki. K, Ogawa K,** 1994. Molecular and crystal structure of the anhydrous form of chitosan. Macromolecules **27,** 7601-7605.

**Yumc, Skipper L, Tannenbaum SR, Chan KK, Ross RK.** 2002. Arylamine Exposures and Bladder Cancer Ris. Nutat. Res. Fun. Mol. M **506-507,** 1-8.

**Zaitsev VS, Filimonov DS, Presnyakov IA, Gambino RJ, Chu B.** 1999. Physical and chemical properties of magnetite and magnetite-polymer nanoparticles and their colloidal dispersions. J Colloid Interf. Sci. **212,** 49-57.

**Zhao D, Zhou J, Liu N.** 2006. Preparation and characterization of *Mingguang palygorskite* supported with silver and copper for antibacterial behavior. Appl. Clay. Sci. **33,** 161-170.